Journal of Thermal Analysis and Calorimetry (2019) 137:659–666
https://doi.org/10.1007/s10973-018-7977-1

Energy and exergy analysis of solar energy-integrated, geothermal energy-powered Organic Rankine Cycle

Merve Senturk Acar[1] · Oguz Arslan[1]

Received: 19 June 2018 / Accepted: 14 December 2018 / Published online: 2 January 2019

Abstract

In this study, the energy and exergy analysis of the solar- and geothermal energy-powered Organic Rankine Cycle was made for different system configurations and Simav geothermal field was taken into consideration for system designs. The solar collectors were integrated into the system with thermal energy storage tank. The R-600a, Therminol VP-1, and molten salt were used as a working fluid in Organic Rankine Cycle, solar field, and thermal energy storage, respectively. As a result of this study, the energy and exergy efficiencies of the geothermal-powered ORC were decreased with the integration of solar energy. But the net power output of the system was increased. The energy and exergy efficiencies of the solar energy-aided, geothermal-powered Organic Rankine Cycle increase by the decrease in the solar collector area. The energy generation of the proposed system was calculated up to 305,713.5 kWh.

Keywords Organic Rankine Cycle—ORC · Solar · Geothermal · Energy · Exergy

List of symbols

A_{Coll}	Total collector area (m^2)
c	Specific heat (kJ kg^{-1} K^{-1})
$\dot{E}x$	Exergy (kW)
H	Specific enthalpy (kJ kg^{-1})
I	Solar radiation (W m^2)
$\dot{m}$	Mass flow (kg s^{-1})
$\dot{Q}$	Heat energy (kJ s^{-1})
T	Temperature (K)
$\dot{W}$	Power (kJ s^{-1})
ε	Exergy efficiency (%)
ψ	Specific exergy (kJ kg^{-1})
η	Energy efficiency (%)

Subscripts

Coll	Solar collector
G	Generator
Gf	Geothermal fluid
HE	Heat exchanger
m,i	Inlet mass flow
m,o	Outlet mass flow
P	Pump
Wf	Working fluid
T	Turbine
TES	Thermal energy storage unit

✉ Oguz Arslan
oguz.arslan@bilecik.edu.tr

Merve Senturk Acar
merve.senturkacar@bilecik.edu.tr

[1] Mechanical Engineering Department, Engineering Faculty, Bilecik Seyh Edebali University, Bilecik, Turkey

Introduction

As a result of the rapid increase in the population and the technological developments in our country and the world, the environmental impacts and sustainability of the energy sources are becoming more important. In this regard, the use of renewable energy resources in energy conversion systems is increasing [1–4]. Turkey has a good condition with its renewable energy sources such as wind, geothermal, and solar energy. Simav geothermal field is one of the usable energy sources. Geothermal heat sources with low temperature are used with binary cycles since the electricity conversion efficiency is higher than the steam power plants [5]. The Organic Rankine Cycle (ORC) is the one type of the binary cycle which is used an organic working fluid [6].

In the literature, the power plants cycle types were analyzed according to resources to the energy and exergy

analysis [7, 8]. Luo et al. [7] analyzed the energy efficiencies of the single-flash and binary cycle by using mid–low-temperature geothermal resource and waste heat resource. They stated that if the energy resource water temperature is higher than 403.15 K, the flash steam power plant is more effective than a binary cycle. Yari [8] investigated the energy and exergy efficiencies of the single-flash, double-flash and flash-binary, simple ORC, ORC with an internal heat exchanger, regenerative ORC, and regenerative ORC with an internal heat exchanger geothermal power plants for three working fluids (R-113, R-123, and n-Pentane). The results show that the exergy destruction in the single-flash plant is higher than the double-flash and flash-binary plants. The energy efficiencies of the binary cycles changed between 6.362 and 15.35%. It is mentioned that the highest energy efficiency is obtained for the binary cycle with a regenerative ORC with an internal heat exchanger and R-123 as the working fluid. Basaran and Ozgener [9] investigated the energy and exergy efficiencies of the binary geothermal power plant for twelve different working fluids. As a result of the thermodynamical analysis, they mentioned that the dry-type fluids (R-236ea, R-600, R-600a, R-227ea) are more efficient than the wet-type fluids (R-143a, R-415A, R-290, R 413A). Heberle and Brüggemann [10] investigated the most effective working fluid for combined geothermal energy power and heat cycle according to the exergy analysis. They mentioned that the isobutane and R-227ea were efficient working fluids for series circuit and parallel circuit, respectively. Zhou et al. [11] investigated the hybrid solar–geothermal power plants for Australian geological and climatic conditions by using the economic and exergy analysis. They mentioned that the hybrid solar–geothermal power plants have more potential and economic benefits than stand-alone geothermal and stand-alone solar power plants. The results showed that the net power output value of the geothermal–solar power plant is higher than the stand-alone ORC [12, 13]. Arslan and Yetik [14] optimized supercritical ORC-binary cycle by using artificial neural network (ANN). Some studies have investigated the performance of the power plants [15–17].

Sonsaree et al. [18] and Cioccolanti et al. [19] investigated the performance of a small-scale solar ORC plant. Nouri et al. [20] analyzed the combined heat and power system with Brayton, Rankine, and ORC from the viewpoint of energy and exergy. Sheshpoli et al. [21] analyzed the waste heat recovery from a hybrid system using recuperative ORC. They used two different working fluids and waste heat of hybrid vapor compression refrigeration cycle and fuel cell for analyses. Sadeghi et al. [22] used a modified artificial bee colony algorithm for the performance analysis and optimization of ORC.

In this study, the solar energy-aided ORC for energy production from geothermal energy in Simav was compared with geothermal-powered ORC. The solar energy-aided, geothermal-powered ORC and geothermal-powered ORC were evaluated by means of energy and exergy analysis from the thermodynamics point of view.

Simav geothermal field

Simav geothermal field is located in the southern part of the Simav graben system (39 latitude, 28 .4′ longitude) at Kutahya province in western Anatolia of Turkey. And it is one of the most important geothermal fields in Turkey. The wellhead temperature is up to 420.85 K in the Simav geothermal field. Between 1985 and 2008, General Directorate of Mineral Research and Exploration (MTA) has drilled ten deep wells ranging in depth from 169 to 725 m [14, 15, 23, 24]. Simav geothermal field and wells' location in the field are shown in Fig. 1. Well properties of Simav geothermal region are given in Table 1.

Design of solar and geothermal energy integrated Organic Rankine Cycle

Geothermal-powered ORC integrated solar energy system is given in Fig. 2. As shown in Fig. 1, the solar energy was integrated into the ORC through the thermal energy storage (TES) tank. Thus, the solar energy was given the ORC with the aid of TES whole day equally. The Therminol VP-1 and molten salt were used as working fluid in solar tube collector and TES, respectively. The thermodynamic properties of Therminol VP-1 and molten salt were calculated using the thermodynamic properties equations in the literature [25]. The heat of geothermal energy was transferred to the working fluid with the heat exchanger (H.E. 1). The heated working fluid enters the heat exchanger (H.E. 2) and takes the heat of salt. Then, the working fluid enters the turbine where power is produced. It enters the air-cooled condenser and leaves as the saturated liquid. The R-600a was used as a working fluid in ORC. The ORC parameters are designed parametrically according to the geothermal energy heat source temperature. The properties of the system units and system parameters are given in Tables 2 and 3. The thermodynamic properties of R-600a were determined by Reference Fluid Thermodynamic and Transport Properties Database (REFPROP) [26]. The solar radiation values of Simav were calculated by using global radiation values of Simav (Kutahya). The global radiation values for Simav region were used in the study. These values in monthly basis are given in Table 4 [28].

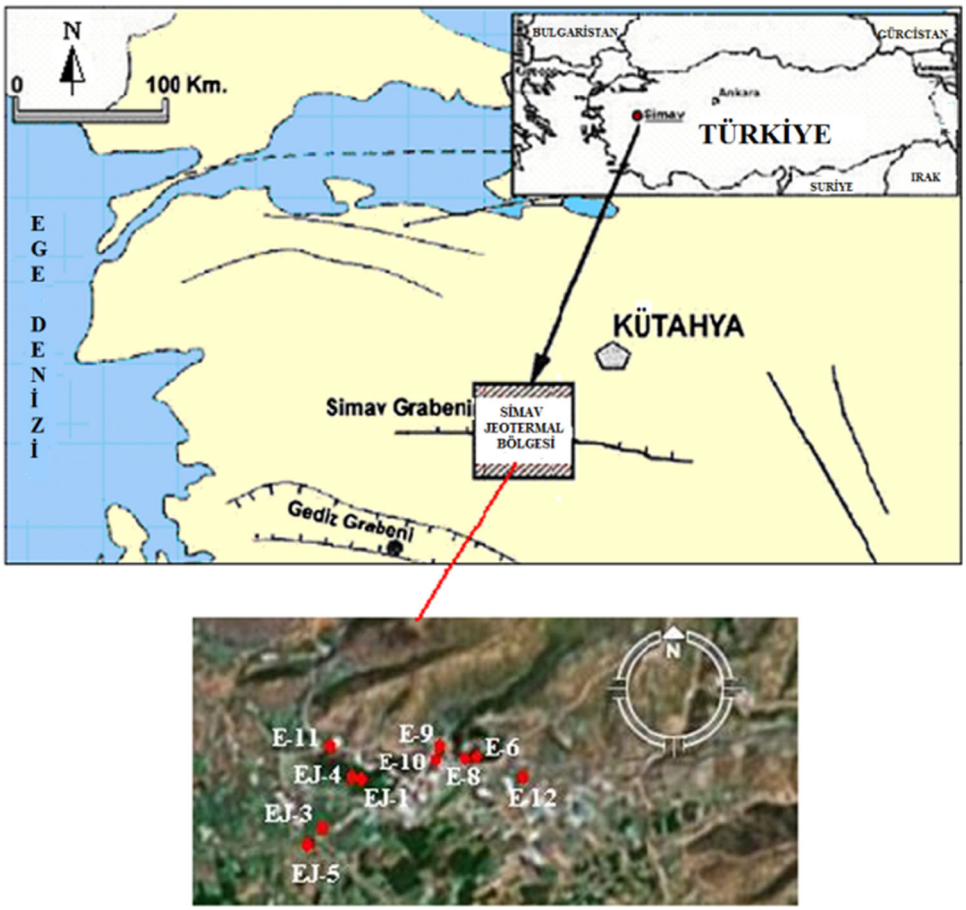

Fig. 1 Location of the Simav geothermal fields and wells [14, 15, 23, 24]

Table 1 Well properties of Simav geothermal region [14, 15, 23, 24]

	$\dot{m}_{gf}$/kg s^{-1}	T_{gf}/K
Ej-1	72	420.85
Ej-3	50	412.05
Ej-4	65	412.05
Ej-5	60	412.05
E-6	70	412.05
E-8	50	416.75
E-9	60	366.75
E-11	35	361.45

Method

There are some assumptions such as kinetic and potential energy effects are negligible and the reference state is 298.15 K and 101.325 kPa in the thermodynamic analysis. The governing energy equations of the geothermal and solar energy integrated ORC were obtained as follows:

The rate of useful heat is gained for the collector [27];

$$\dot{Q}_{Coll} = I \cdot A_{Coll} \cdot \eta_{Coll} \tag{1}$$

The rate of heat transfer input from the sun is given by;

$$\dot{Q}_{sun} = \frac{\dot{Q}_{Coll}}{\eta_{Coll}} \tag{2}$$

Mass of the heat transfer fluid is calculated as;

$$\dot{m}_{terminol} = \frac{\dot{Q}_{Coll}}{(T_{3b} - T_{3a}) \cdot c_{p,terminol}} \tag{3}$$

The power output of the turbine can be calculated as;

$$\dot{W}_T = \dot{m}_{wf} \cdot (h_{2b} - h_{2a}) \tag{4}$$

The electric power of the generator can be calculated as;

$$\dot{W}_G = \eta_G \cdot \dot{W}_T \tag{5}$$

The power consumption occurring in the pump can be calculated as;

$$\dot{W}_P = \dot{m}_{wf} \cdot (h_{2d} - h_{2c}) \tag{6}$$

The energy of the geothermal heat exchanger is given by;

$$\dot{Q}_{gf} = \dot{m}_{gf} \cdot (h_{1b} - h_{1a}) \cdot \eta_{HE,1} = \dot{m}_{wf} \cdot (h_{2e} - h_{2d}) \tag{7}$$

The energy balance of the salt heat exchanger can be calculated by;

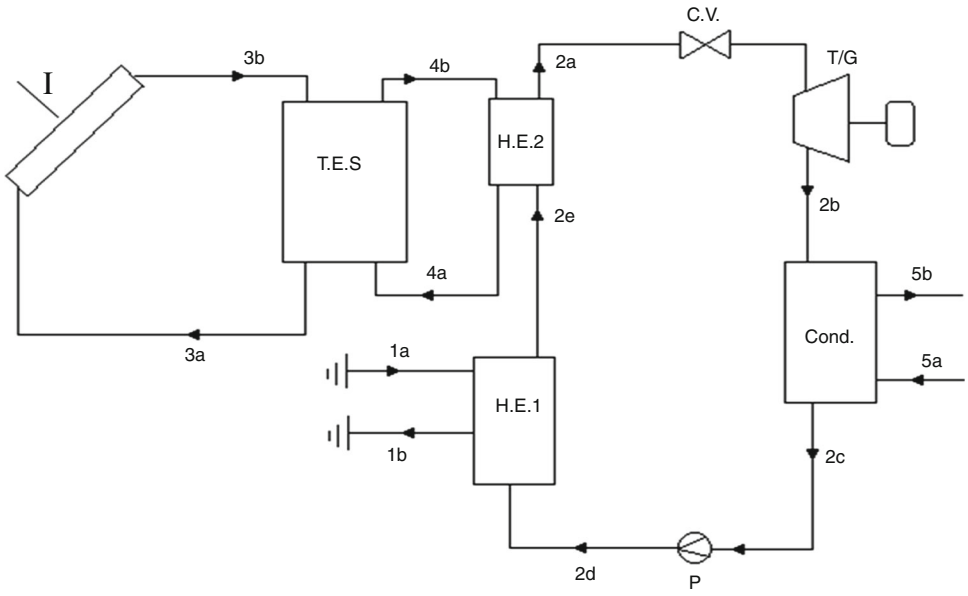

Fig. 2 The flow diagram of the solar and geothermal-powered ORC

Table 2 Properties of system units [23, 25, 27]

Unit	Efficiency
η_{TES}	0.98
η_T	0.85
η_{Coll}	0.85
η_G	0.99
η_P	0.90
η_{HE}	0.98
A_{coll}/m^2	10,000–15,000–20,000
wf	R-600a

Table 3 System parameters

Parameter	Value
T_{1a}/K	406.65
P_{1a}/kPa	300
T_{1b}/K	333.15- 343.15- 353.15- 363.15
T_{2b}/K	313.58
P_{2b}/kPa	323
T_{2c}/K	295.15
T_{2d}/K	296.51
T_{2e}/K	390.15-380.15-370.15
P_{2e}/kPa	2693.9- 2258-1878
T_{3a}/K	568.15
T_{3b}/K	593.15
T_{4a}/K	543.15
T_{4b}/K	588.15
T_{5a}/K	288.15
T_{5b}/K	278.15

$$\dot{m}_{salt} \cdot (h_{4b} - h_{4a}) \cdot \eta_{HE,2} = \dot{m}_{wf} \cdot (h_{2e} - h_{2d}) \tag{8}$$

The net power output of the system is given as;

$$\dot{W}_{net} = \dot{W}_G - \dot{W}_P \tag{9}$$

The energy efficiency of the system is calculated as;

$$\eta = \frac{\dot{W}_{net}}{\dot{Q}_s + \dot{Q}_{gf}} \tag{10}$$

The exergy balance equation for steady systems is given by the following equation:

$$\dot{E}_{X_{heat}} - \dot{E}_{X_{work}} + \dot{E}_{X_{m,i}} - \dot{E}_{X_{m,o}} = \dot{E}_{X_{dest}} \tag{11}$$

where the exergy terms occurred by heat, work, solar radiation exergy, and mass flow are given as follows [27]:

$$\dot{E}_{X_{heat}} = \sum \left(1 - \frac{T_0}{T_k}\right) \cdot \dot{Q}_k \tag{12}$$

$$\dot{E}_{X_{work}} = \dot{W} \tag{13}$$

$$\dot{E}x_s = A_{Coll} \cdot I \cdot \left(1 + (1/3) \cdot (T_0/T_{sun})^4 - (4/3) \cdot (T_0/T_{sun})\right) \tag{14}$$

$$\dot{E}_{X_{m,i}} = \sum \dot{m}_i \cdot \psi_i \tag{15}$$

$$\dot{E}_{X_{m,o}} = \sum \dot{m}_o \cdot \psi_o \tag{16}$$

here, ψ indicates the physical exergy term and is given as:

Table 4 The global radiation values of Simav [28]

Month	Global radiation/kWh m^{-2} day^{-1}
January	1.77
February	2.36
March	3.75
April	4.93
May	6.08
June	6.48
July	6.38
August	5.72
September	4.69
October	3.28
November	2.04
December	1.51

$$\psi = (h - h_0) - T_0 \cdot (s - s_0) \tag{17}$$

where h is enthalpy, s is entropy, and the subscript zero indicates properties of fluids at the dead state. The sun temperature (T_{sun}) is 5800 K [2].The exergetic efficiency of the system is then calculated by the following equation;

$$\varepsilon = 1 - \frac{\dot{E}_{X_{m,total}}}{\dot{E}_{X_{m,i}}} = \frac{\dot{W}_{net}}{(A_{Coll} \cdot I \cdot \psi_s) + \left(\dot{m}_{gf} \cdot (\psi_{1a} - \psi_{1b})\right)} \tag{18}$$

Results and discussion

Handling the operating parameters as T_{2e} = 390 K, A_{coll} = 10,000 m^2, R-600a, the change of the energy efficiency (η) with different geothermal fluid outlet temperatures was obtained as shown in Fig. 3.

Figure 3 shows that the energy efficiency values of the solar energy-aided, geothermal-powered ORC increase by the decrease in the T_{1b}. The energy efficiency of the proposed system ranges between 14.52 and 14.54%. The energy efficiency of geothermal power plant is constant at 14.56%, while the T_{1b} value is increasing. Taking T_{1b} = 353.15 K, T_{2e} = 390.15 K, the change of energy efficiency (η) with different solar collector areas (A_{coll}) was obtained as shown in Fig. 4.

Figure 4 shows that the energy efficiency values of the solar energy-aided, geothermal-powered ORC increase by the decrease in the solar collector area (A_{coll}). The energy efficiency of the proposed system ranges between 14.50 and 14.53%. Taking T_{1b} = 353.15 K, A_{coll} = 10,000 m^2, the change of energy efficiency (η) with the working fluid temperature after the first heat exchanger (T_{2e}) was obtained as shown in Fig. 5.

Figure 5 shows that the energy efficiency values of the solar energy-aided, geothermal-powered ORC increase by the increase in working fluid temperature after the first heat exchanger (T_{2e}). The energy efficiency of the proposed system ranges between 12.56 and 14.56%. The highest energy efficiency value is calculated for the geothermal-powered ORC. For the same system parameters, the energy efficiency value of the solar energy-aided, geothermal-powered ORC is calculates as 14.53%. Taking T_{2e} = 390 K, A_{coll} = 10,000 m^2, the change of exergy efficiency (ε) with different geothermal fluid outlet temperatures was obtained as shown in Fig. 6.

Figure 6 shows that the exergy efficiency values of the solar energy-aided, geothermal-powered ORC and geothermal-powered ORC increase by the decrease in the T_{1b}. The exergy efficiency of the proposed system ranges between 58.24 and 70.91%. Taking T_{1b} = 353.15 K, T_{2e} = 390.15 K, the change of exergy efficiency (ε) with different solar collector areas (A_{coll}) was obtained as shown in Fig. 7.

Figure 7 shows that the exergy efficiency values of the solar energy-aided, geothermal-powered ORC increase by the decrease in the solar collector area (A_{coll}). The exergy

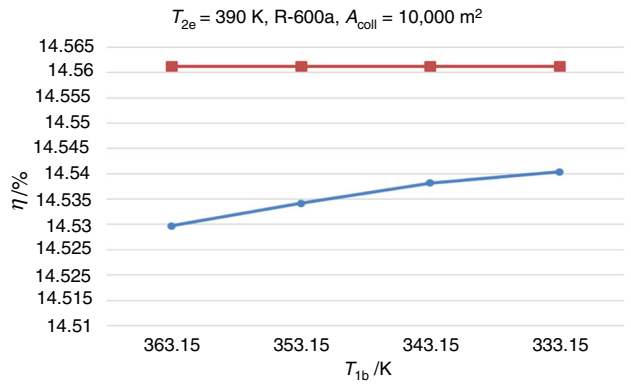

Fig. 3 The variation of η versus T_{1b}

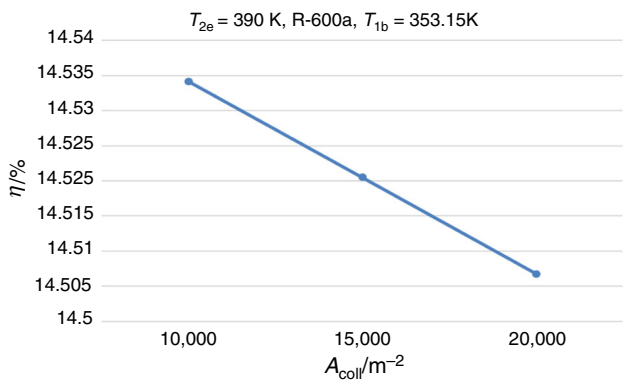

Fig. 4 The variation of η versus A_{coll}

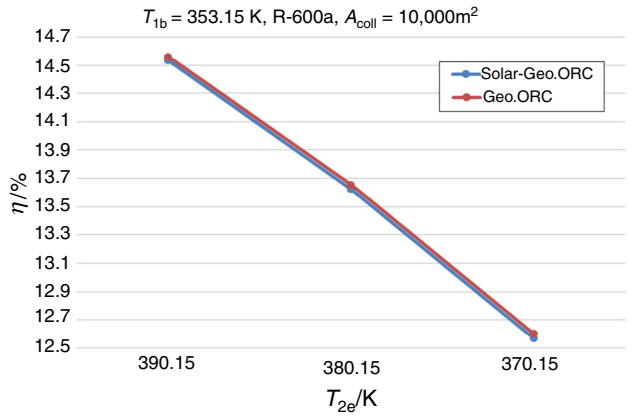

Fig. 5 The variation of η versus T_{2e}

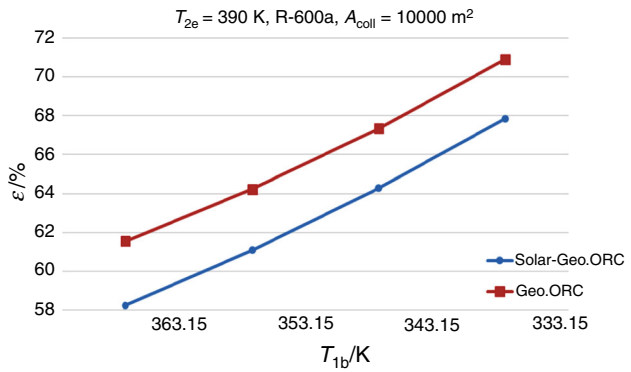

Fig. 6 The variation of ε versus T_{1b}

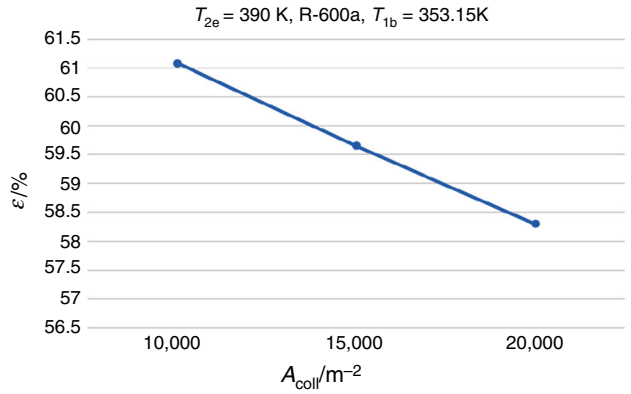

Fig. 7 The variation of ε versus A_{coll}

efficiency of the proposed system ranges between 58.30 and 61.08%. Taking T_{1b} = 353.15 K, A_{coll} = 10,000 m^2, the change of exergy efficiency (ε) with the working fluid temperature after the first heat exchanger (T_{2e}) was obtained as shown in Fig. 8.

Figure 8 shows that the exergy efficiency values of the solar energy-aided, geothermal-powered ORC increase by the increase in working fluid temperature after the first heat exchanger (T_{2e}). The exergy efficiency of the proposed

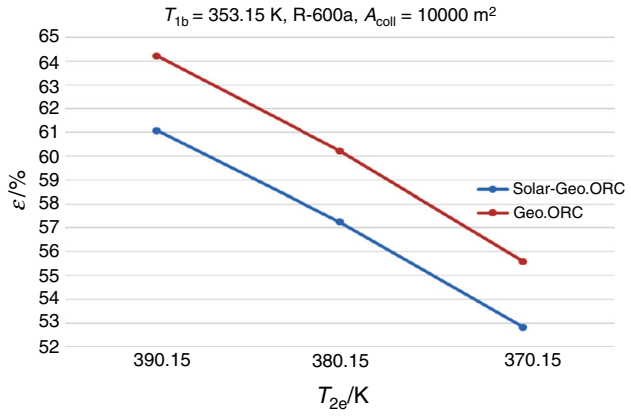

Fig. 8 The variation of ε versus T_{2e}

system ranges between 52.81 and 64.22%. The highest exergy efficiency value is calculated for the geothermal-powered ORC as 64.22%. For the same system parameters, the exergy efficiency value of the solar energy-aided, geothermal-powered ORC is calculates as 61.08%. Taking T_{1b} = 353.15 K, A_{coll} = 10,000 m^2, the change of net energy production of the systems with the working fluid temperature after the first heat exchanger (T_{2e}) was obtained as shown in Fig. 9.

Figure 9 shows that the net electrical energy production values of the solar energy-aided, geothermal-powered ORC increase by the increase in working fluid temperature after the first heat exchanger (T_{2e}). The net electrical energy production of the proposed system ranges between 146,362 and 171,385 kWh. The highest net electrical energy production value is calculated for solar energy-aided, geothermal-powered ORC. For the same system parameters, the net electrical energy production value of the geothermal-powered ORC is calculated as 169,128 kWh.

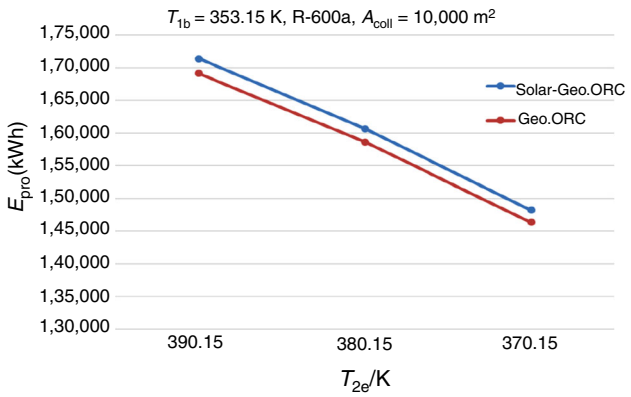

Fig. 9 The variation of E_{pro} versus T_{2e}

Conclusions

In this study, the solar- and geothermal energy-powered ORC was designed by using the well properties of Simav geothermal field. The net power output, energy, and exergy efficiencies of the geothermal-powered ORC and solar-integrated, geothermal-powered ORC were determined. The solar energy was integrated into the power plant using a thermal energy storage unit.

The most effective system parameters were determined as T_{1b} = 333.15 K, T_{2e} = 390.15 K, and A_{coll} = 10,000 m^2. The electrical and exergetic efficiencies of the solar energy-aided, geothermal-powered ORC were calculated as 14.54% and 67.84%, respectively. For the same conditions, the electrical and exergetic efficiency of the geothermal-powered ORC was calculated as 14.56% and 70.91%, respectively. The net electrical energy production of the solar energy-aided, geothermal-powered ORC and the geothermal-powered ORC was calculated as 302,575.1 kWh and 305,713.5 kWh, respectively. The decrease in energy efficiencies of solar- and geothermal-powered ORC, in comparison with the energy efficiencies of geothermal-powered ORC, changes between 0.02 and 0.04%. These decrease ratios for the exergy efficiencies were determined as between 2.76 and 5.92%. By the integration of the solar energy to the power cycle, the net electrical energy production increases in a range between 1.03% and 1.3%.

The obtained results show that it is not possible to decide whether the installation of the solar-integrated system is efficient or not. Because the change between the two handled system efficiencies is relatively small. Besides, the net power output value of the solar-integrated, geothermal-powered ORC is higher than a geothermal-powered ORC.

Since solar energy is a renewable energy source, there is no payment for energy source during the lifetime of the system and it also has no effect on the environment. Therefore, it can be taken into consideration to invest for a system such that. However, it would be better to decide by using different analysis methods which design is the best. For this aim, economic analysis of the proposed systems should be performed. The determination of levelized cost of energy seems as a good choice in which the costs of operating, maintenance, installation, and selvage are included.

References

1. Tugcu A, Arslan O. Thermodynamics and economical analysis of geothermal assisted absorption refrigeration system: Simav case study. J Therm Sci Technol. 2016;36:143–59.
2. Tempesti D, Manfrida G, Fiaschi D. Thermodynamic analysis of two micro CHP systems operating with geothermal and solar energy. Appl Energy. 2012;97:609–17.
3. Tempesti D, Fiaschi D. Thermo-economic assessment of a micro CHP system fuelled by geothermal and solar energy. Energy. 2013;58:45–51.
4. Ezzat MF, Dincer I. Energy and exergy analyses of a new geothermal–solar energy based system. Sol Energy. 2016;134:95–106.
5. Valdimarsson P. Geothermal Power Plant Cycles and Main Components, Short Course on Geothermal Drilling, Resource Development and Power Plants; 2011, p. 16–22. "Short Course on Geothermal Drilling, Resource Development and Power Plants", organized by UNU-GTP and LaGeo, in Santa Tecla, El Salvador, 16–22 Jan 2011.
6. Walraven D, Laenen B, D'haeseleer W. Comparison of thermodynamic cycles for power production from low-temperature geothermal heat sources. Energy Convers Manag. 2013;66:220–33.
7. Luo C, Huang L, Gong Y, Ma W. Thermodynamic comparison of different types of geothermal power plant systems and case studies in China. Renew Energy. 2012;48:155–60.
8. Yari M. Exergetic analysis of various types of geothermal power plants. Renew Energy. 2010;35:112–21.
9. Basaran A, Ozgener L. Investigation of the effect of different refrigerants on performances of binary geothermal power plants. Energy Convers Manag. 2013;76:483–98.
10. Heberle F, Brüggemann D. Exergy based fluid selection for a geothermal Organic Rankine Cycle for combined heat and power generation. Appl Therm Eng. 2010;30:1326–32.
11. Zhou C, Doroodchi E, Moghtaderi B. An in-depth assessment of hybrid solar-geothermal power generation. Energy Convers Manag. 2013;74:88–101.
12. Ghasemi H, Sheu E, Tizzanini A, Paci M, Mitsos A. Hybrid solar-geothermal power generation: optimal retrofitting. Appl Energy. 2014;131:158–70.
13. Zhou C. Hybridisation of solar and geothermal energy in both subcritical and supercritical Organic Rankine Cycles. Energy Convers Manag. 2014;81:72–82.
14. Arslan O, Yetik O. ANN based optimization of supercritical *ORC*-Binary geothermal power plant: Simav case study. Appl Therm Eng. 2011;31:3922–8.
15. Arslan O. Exergoeconomic evaluation of electricity generation by the medium temperature geothermal resources, using a Kalina Cycle: Simav case study. Int J Therm Sci. 2010;49:1866–73.
16. Boukelia TE, Arslan O, Mecibah MS. ANN-based optimization of a parabolic trough solar thermal power plant. Appl Therm Eng. 2016;107:1210–8.
17. Boukelia TE, Arslan O, Mecibah MS. Potential assessment of a parabolic trough solar thermal power plant considering hourly analysis: ANN-based approach. Renew Energy. 2017;105:324–33.
18. Sonsaree S, Asaoka T, Jiajitsawat S, Aguirre H, Tanaka K. A small-scale solar Organic Rankine Cycle power plant in Thailand: three types of non-concentrating solar collectors. Sol Energy. 2018;162:541–60.
19. Cioccolanti L, Tascioni R, Arteconi A. Mathematical modelling of operation modes and performance evaluation of an innovative small-scale concentrated solar organic Rankine cycle plant. Appl Energy. 2018;221:464–76.
20. Nouri M, Namar MM, Jahanian O. Analysis of a developed Brayton cycled CHP system using *ORC* and CAES based on first and second law of thermodynamics. J Therm Anal Calorim. 2018. https://doi.org/10.1007/s10973-018-7316-6.
21. Sheshpoli MA, Ajarostaghi SSM, Delavar MA. Thermodynamic analysis of waste heat recovery from hybrid system of proton

exchange membrane fuel cell and vapor compression refrigeration cycle by recuperative organic Rankine cycle. J Therm Anal Calorim. 2018. https://doi.org/10.1007/s10973-018-7338-0.
22. Sadeghi S, Maghsoudi P, Shabani B, Gorgani HH, Shabani N. Performance analysis and multi-objective optimization of an organic Rankine cycle with binary zeotropic working fluid employing modified artificial bee colony algorithm. J Therm Anal Calorim. 2018. https://doi.org/10.1007/s10973-018-7801-y.
23. Arslan O. Ultimate evaluation of Simav-Eynal geothermal resources: design of integrated system and its energy-exergy analysis. Ph.D. thesis. Eskisehir: Eskisehir Osmangazi University. Institute of Applied Sciences; 2008 **(in Turkish)**.
24. Arat H, Arslan O. Exergoeconomic analysis of district heating system boosted by the geothermal heat pump. Energy. 2017;119:1159–70.
25. Li X, Xu E, Song S, Wang X, Yuan G. Dynamic simulation of two-tank indirect thermal energy storage system with molten salt. Renew Energy. 2017;113:1311–9.
26. REFPROP, NIST Reference Fluid Thermodynamic and Transport Properties. NIST Reference Database. Version 9.0, National Institute of Standards and Technology USA; 2010.
27. Aydin D, Utlu Z, Kıncay O. Thermal performance analysis of a solar energy sourced latent heat storage. Renew Sustain Energy Rev. 2015;50:1213–25.
28. Potential atlas of solar energy. Republic of Turkey Ministry of Energy and Natural Resources. 2018. http://www.yegm.gov.tr/MyCalculator. Accessed Jan 2018.